

See discussions, stats, and author profiles for this publication at: <https://www.researchgate.net/publication/261215491>

Casein Phosphopeptide–Biofunctionalized Graphene Biocomposite for Hydroxyapatite Biomimetic Mineralization

ARTICLE · MAY 2013

DOI: 10.1021/jp312163m

CITATIONS

12

READS

60

10 AUTHORS, INCLUDING:



Fan Zengjie

Technical Institute of Physics and Chemistry

13 PUBLICATIONS 180 CITATIONS

[SEE PROFILE](#)



Jinqing Wang

Chinese Academy of Sciences

103 PUBLICATIONS 1,805 CITATIONS

[SEE PROFILE](#)



Zhaofeng Wang

Chinese Academy of Sciences

63 PUBLICATIONS 721 CITATIONS

[SEE PROFILE](#)



Peiwei Gong

Chinese Academy of Sciences

27 PUBLICATIONS 303 CITATIONS

[SEE PROFILE](#)

Casein Phosphopeptide-Biofunctionalized Graphene Biocomposite for Hydroxyapatite Biomimetic Mineralization

Zengjie Fan,^{†,‡} Jinqing Wang,^{*,†} Zhaofeng Wang,[†] Zhangpeng Li,[†] Yinong Qiu,[§] Honggang Wang,[†] Ye Xu,^{†,‡} Lengyuan Niu,^{†,‡} Peiwei Gong,^{†,‡} and Shengrong Yang^{*,†}

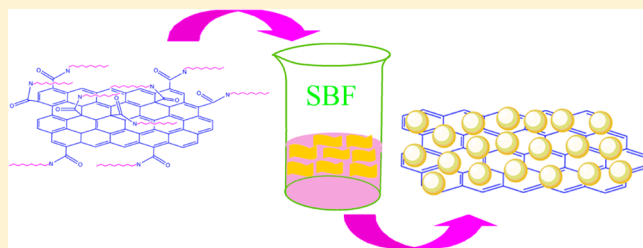
[†]State Key Laboratory of Solid Lubrication, Lanzhou Institute of Chemical Physics, Chinese Academy of Sciences, Lanzhou 730000, P. R. China

[‡]University of Chinese Academy of Sciences, Beijing 100080, P. R. China

[§]Department of Stomatology, Lanzhou General Hospital, Lanzhou Command PLA, Lanzhou 730050, P. R. China

Supporting Information

ABSTRACT: Casein phosphopeptides (CPPs) with abundant phosphoserine clusters can mediate hydroxyapatite (HA) nucleation and growth. In this work, a new type of CPPs-biofunctionalized graphene composite was synthesized by amidation reaction between CPPs and carboxylated graphene (CGO). When immersed in stimulated body fluid (1.5 × SBF) at 37 °C for different periods, the CPPs layer on the composite facilitated efficient interaction between the CGO surface and mineral ions, which promoted HA nanoparticle formation and shortened mineralization time in comparison with pristine CGO. The synthesis of the composite mimicked the natural biomineratization of bone, demonstrating that CPPs can effectively improve the bioactivity of graphene and be useful for HA formation. The presented biocomposite may have potential biomedical applications in different areas.



mineralized growth by a biocompatible aqueous solution under mild conditions, and the resulting HA is found to be similar to the mineral in natural bone.¹⁸ Biomineratization involves the initial nucleation and subsequent growth of HA from aqueous solutions; however, inert materials are difficult to be mineralized by the biomimetic method without surface modification.¹⁹ In general, the surface functional groups of the materials play a decisive role in both nucleation and growth. Some reports revealed that the introduction of functional groups such as proteins,²⁰ dopamine,²¹ peptide fibers,²² and amino acid²³ as calcium ions nucleation sites can promote HA formation when immersed in stimulated body fluid (SBF) that contains ion concentrations nearly equal to those of human blood plasma.²⁴

Graphene, being the thinnest and strongest material ever produced, is viable as a reinforcement or filling material for tissue engineering because of its high theoretical tensile strength (150 GPa) and Young's modulus (1.0 TPa).²⁵ As an inert material, graphene cannot be mineralized in SBF by the biomimetic method because its surface lacks functional groups, thereby limiting its extensive application as a bone-grafting material.²⁶ Some studies found that the introduction of phosphate groups on the surface of inert materials can mimic nucleation and induce HA mineralization.^{27,28} Casein phos-

INTRODUCTION

Hydroxyapatite (HA) is an important inorganic material found in hard tissues of bone and teeth. HA can be widely applied in orthopedic, dental, and maxillofacial fields because of its excellent biocompatibility and bioactivity with the human tissue.^{1,2} Nevertheless, poor tensile strength and fracture toughness limit its extensive applications.^{3,4} Some inert materials with excellent mechanical property, such as titanium,⁵ titanium alloy,^{4,6} carbon nanotube,^{7,8} and graphene,⁹ can be employed to toughen and strengthen HA. In bone grafting, these composite materials are commonly used to replace damaged or missed bone tissues. However, the above-mentioned filling materials cannot bind to the surrounding tissues tightly when they are implanted in the human body without any special treatment, leading to the separation between the implanted material and host tissues.¹⁰ The formation of bone-like apatite on their surfaces is necessary for artificial materials to make direct bond with living bone.¹¹ HA coating can improve fixation between hard tissues and metal implants. In addition, synthetic HA is a biocompatible prosthetic material that can strongly bond to the bone and promote the formation of bone tissue on its surface.¹²

Methods such as hydrothermal reaction,¹³ sol-gel synthesis,¹⁴ precipitation methods,¹⁵ and plasma-sprayed synthesis¹⁶ have been developed to prepare HA coating directly on the surface of inert materials. Aside from these methods, biomimetic mineralization is another powerful candidate for the synthesis of HA.¹⁷ This process can mimic the biologically

Received: December 10, 2012

Revised: March 12, 2013

Published: April 29, 2013



phopeptides (CPPs) with abundant phosphoserine clusters are important bioactive and biocompatible peptides involved in various physiological regulation processes.²⁹ As a primary structure of protein, phosphate groups on CPPs are exposed on the surface, creating a polar, acidic domain more favorable for binding divalent calcium ions.²⁹ CPPs are easily obtained and very cheap.³⁰ Therefore, they can be used as nucleation sites for binding calcium ions and promoting HA formation. However, relevant reports on the application of CPPs in modifying graphene and promoting its mineralization in virtue of the biomimetic method remain lacking to date. Accordingly, the present paper focuses on modifying graphene with CPPs to improve its bioactivity and promote mineralization in SBF.

In this work, we successfully synthesized a CGO–CPPs biocomposite scaffold. The as-prepared scaffold was immersed in SBF solution for different periods to mimic natural mineralization. The synthesized CGO–CPPs composite may serve as a new scaffold for synthesizing HA coating on its surface and for improving graphene bioactivity. The obtained material may have potential applications in the fields of bionanotechnology and biomedicine.

EXPERIMENTAL SECTION

Reagents and Materials. CPPs, 1-ethyl-3-(3-dimethylaminopropyl) carbodiimide hydrochloride (EDCA), and *N*-hydroxysuccinimide (NHS) were purchased from Sigma. Graphite powder (99.95%, 325 mesh) was obtained from Sinopharm Chemical Reagent. Sodium chloroacetate ($\text{ClCH}_2\text{COONa}$) was purchased from Tianjin Reagent Factory. Unless otherwise stated, other reagents were of analytical grade and used as received. All aqueous solutions were prepared with Milli-Q ultrapure water (>18 M Ω ·cm).

Preparation of CGO–CPPs Biocomposite. GO colloid was prepared by a modified Hummers method using graphite powder as starting material.³¹ CGO was obtained according to a previously described method with slight modifications.³² First, GO (100 mg) was dispersed in ultrapure water (100 mL). Then, NaOH (5 g, 125 mmol) and $\text{ClCH}_2\text{COONa}$ (5 g, 42.9 mmol) were added. The resulting reaction mixture was sonicated for 2 h to form CGO, which was purified by repeated rinsing and collected by centrifugation. The sediment was redispersed in 60 mL of 0.1 M phosphate buffer solution (pH 7.0). In the conjugation of CGO with the peptide, 5 mM NHS and 1 mM EDCA were added into the CGO suspension. The mixture was bath-sonicated for 1 h, adjusted to pH 8.0 with 1 mM NaOH, and then added with 1.5 mM CPPs. The mixture was stirred vigorously at 37 °C in the dark overnight. The product was purified by repeated centrifugation at 12 000 rpm for 30 min and then rinsed with ultrapure water to remove the unreacted peptides. The final product was frozen at -55 °C for 2 h and then dried by sublimation in a vacuum chamber for 24 h. The dry sample was stored in a refrigerator at 4 °C for further study.

Biomineralization. To accelerate HA formation, we prepared a solution with 1.5 times ionic concentrations of SBF ($1.5 \times \text{SBF}$). The composition of $1.5 \times \text{SBF}$ was listed as follows: Na^+ , 213.0 mM; K^+ , 7.5 mM; Mg^{2+} , 2.25 mM; Ca^{2+} , 3.75 mM; Cl^- , 221.7 mM; HCO_3^- , 6.3 mM; HPO_4^{2-} , 1.5 mM; and SO_4^{2-} , 0.75 mM. The samples of CGO and CGO–CPPs were, respectively, immersed in SBF for different periods in a thermostatic bath at 37 °C. Finally, the samples were washed with water and dried at room temperature for further analysis.

Characterization. The morphology, composition, and structure of the synthesized samples were characterized by scanning electron microscopy (SEM, JEOL JSM-6701F), transmission electron microscopy (TEM, JEOL JEM-2010), energy-dispersive X-ray spectroscopy (EDX), X-ray diffraction (XRD, Rigaku D/Max-2400 diffractometer using Cu $\text{K}\alpha$ radiation and graphite monochromator, $\lambda = 1.54056 \text{ \AA}$), Fourier transform infrared spectroscopy (FTIR, Bruker IFS66 V FTIR spectrometer), X-ray photoelectron spectroscopy (XPS, PHI-5702, Physical Electronics, USA, using a monochromated Al $\text{K}\alpha$ irradiation; the chamber pressure was $\sim 3 \times 10^{-8}$ Torr under testing condition), water contact angle measurement (WCA, DSA100, Germany), and thermogravimetric analysis (TGA) under a nitrogen atmosphere with a Perkin-Elmer Thermal Analyzer.

RESULTS AND DISCUSSION

Preparation and Characterization of CGO–CPPs Biocomposite.

The construction of CGO–CPPs biocomposite and the subsequent biomimetic mineralization processes are illustrated in Figure 1. Brown-yellow water-soluble GO with

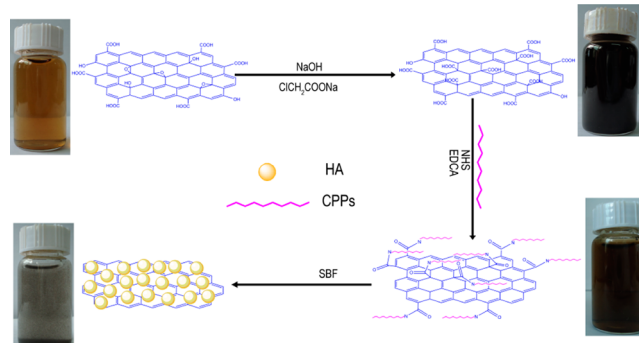


Figure 1. Illustration of the sample preparation and biomimetic mineral processes.

numerous carboxylic, hydroxyl, and epoxide groups on its sheets reacts with $\text{ClCH}_2\text{COONa}$ under strong alkaline conditions to convert the hydroxyl and epoxide groups into carboxylate groups,³³ resulting in a black CGO solution. Compared with GO, CGO has more carboxylic acid groups that are available for subsequent amidation with the aid of EDCA and NHS. CGO can integrate with more CPPs than GO, and more phosphate groups on CPPs mean higher mineralization rate than CGO. After CPPs reacted with CGO, the solution turned from black to brownish black. When the composite was immersed in SBF for certain periods, the composite solution turned dark. As a result, the composite was difficult to be homogeneously dispersed in water because of the HA formation on its surface.

The phase and composition of GO, CGO, and CGO–CPPs were analyzed by XRD (Figure 2). For GO, a sharp and intensive peak appeared at 9.8°, which corresponded to the (001) diffraction of GO.³⁴ Upon carboxylation, two new peaks appeared at 11.5 and 21.2°, whereas the (001) plane of GO disappeared. The binding of CGO with CPPs through amidation gave rise to a broad diffraction peak for CGO–CPPs. This result confirms that the composite has a noncrystalline structure.

The XPS spectra of GO, CGO, and CGO–CPPs are presented in Figure 3. For GO, the C1s spectrum can be

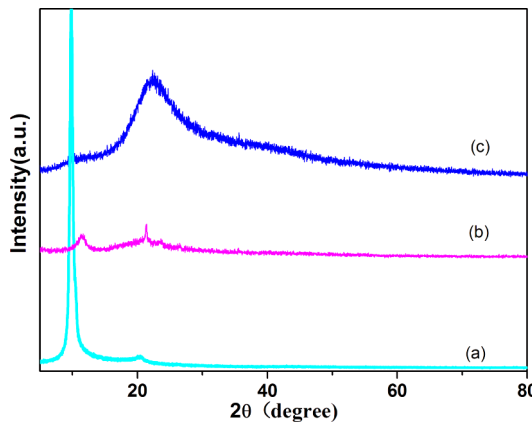


Figure 2. XRD patterns of GO (a), CGO (b), and CGO–CPPs (c).

decomposed into four peaks ranging from 282.0 to 292.0 eV. These peaks were assigned to C=C (284.8 eV), C–O (286.4 eV), C=O (287.8 eV), and HO–C=O (290.8 eV) groups.³⁵ After the carboxylation of GO, the peak at 286.4 eV for the C–O group disappeared. Meanwhile, the peak intensities of C=O and HO–C=O were higher than those in GO. The XPS results indicated that the C–O groups were converted into C=O groups under strong alkaline conditions; that is, the final products were CGO. The XPS survey spectrum of CGO–CPPs identified C, O, and N as the constituting elements. In addition, the appearance of N was attributed to the introduction of CPPs on the composite. The C1 s spectrum of the composite in Figure 3d consisted of four peaks at 284.8, 285.9, 286.6, and 287.6 eV, which corresponded to C=C, C–O, C–N, and C=N=O groups, respectively.³⁶ The C–N=O group was caused by the condensation reaction between amino groups and carboxyl groups. Figure 3e,f provides the high-resolution XPS N 1s and P 2p spectra of CGO–CPPs at 400.2 and 131.2 eV, respectively. The XPS results demonstrated the successful bonding of CPPs with CGO through amidation.

FTIR spectroscopy was further used to characterize the products (Figure 4). Obviously, the FTIR spectra of GO, CGO, and CGO–CPPs displayed a broad band at 3400 cm⁻¹, which corresponded to the O–H stretching vibration of the adsorbed water molecules. The spectrum of GO clearly indicated the presence of oxygen-containing functional groups at 1055, 1227, 1392, 1622, and 1730 cm⁻¹, which corresponded to the C–O stretching vibration, C–OH stretching vibration, C–O–H deformation vibration, C=C stretching vibration, and C=O stretching vibration of COOH groups, respectively.³⁷ In the spectrum of CGO, the band at 1227 cm⁻¹ belonging to C–O groups disappeared, indicating their conversion to carboxyl groups. This result is in accordance with that of XPS analysis, providing strong evidence of carboxylation for GO. Upon the reaction of CPPs with CGO, a strong characteristic band appeared at 1650 cm⁻¹, which can be ascribed to the stretching vibration of –CO–NH–.³⁷ This result indicates the successful conjugation of CPPs with CGO through amidation.

SEM and WCA images of CGO and CGO–CPPs are shown in Figure 5. For CGO (Figure 5a), the flat surface was decorated with some wrinkles, and the WCA of CGO film was 75°. After being modified with CPPs (Figure 5b), the surface became rougher with more obvious wrinkles, and the WCA reduced to 58°. Therefore, the introduction of CPPs can effectively improve the surface roughness and hydrophilicity of CGO, facilitating the improvement of the mineralization rate.

The related discussion is presented in the following section. The TEM image of Figure 5c showed that the surface of CGO was very smooth with a larger wrinkle on the edge, and the EDX pattern indicated that CGO was composed of C and O elements (Supporting Information, Figure S1a). Upon modifying with CPPs (Figure 5d), the sheet became rougher with more wrinkles on the whole composite surface, and a new peak assigned to P element appeared on the EDX pattern (Supporting Information, Figure S1b). Conversely, the transparent sheet turned darker because of the increase in thickness of the sheet after the introduction of CPPs.^{38,39} As a result, light transmittance was reduced, making it appear darker than CGO. TEM results are an effective supplement for SEM observation, further confirming that the synthesized composite is composed of CGO and CPPs.

Bioactivity Evaluation of CGO–CPPs Composite. In vitro test was carried out in 1.5× SBF solution to monitor the deposition of apatite on their surfaces and to evaluate and compare the bioactivity of the prepared CGO and CGO–CPPs samples. SEM images of the biomimetic growth of HA on the surfaces of CGO and CGO–CPPs are shown in Figure 6. After CGO was immersed in SBF for 1 day, the surface of CGO almost had the same morphology as the original CGO, and no obvious deposits were observed (Figure 6a). When the incubation time was prolonged to 3 days, some congregated HA nanoparticles sparsely appeared on its surface (Figure 6b). After 1 day of immersion in SBF, the surface of CGO–CPPs was partially covered by HA nanoparticles with an average diameter of ~50 nm (Figure 6c and Supporting Information, Figure S2a). As the soaking time was prolonged to 3 days, the surface of the composite was completely covered by HA nanoparticles (Figure 6d and Supporting Information, Figure S2b). In addition, the interparticles had tiny pores that facilitate cellular adhesion and growth (Supporting Information, Figure S2b). The above SEM results indicate that the introduction of CPPs can significantly accelerate the formation rate of HA and reduce the mineralization time.

To provide better qualitative understanding of the internal structure and spatial distribution of CGO–CPPs, we used the 3 day sample for the following TEM observation and XPS characterization. As shown in the TEM image of Figure 7a, HA nanoparticles tightly coated the surface of CGO–CPPs. The strong concentric ring in the selected area electron diffraction (SAED) pattern can be indexed as the (002) and (211) diffractions of HA, displaying a polycrystal structure (Supporting Information, Figure S3a). The high-resolution TEM image of the individual particle provided further insights into the nanostructured nature, as shown in Figure 7b, in which the (211) plane of the HA crystal can be identified according to the *d* spacing of ~3.1 Å.⁴⁰ The EDX examination of the sample confirmed the presence of Ca, P, C, and O as the major constituents (Supporting Information, Figure S3b). The XPS survey spectrum of the CGO–CPPs composite (Supporting Information, Figure S4a) showed C 1s, O 1s, N 1s, and P 2p peaks. This result further confirmed the successful binding of CPPs to the surface of CGO. After mineralization in SBF for 3 days (Supporting Information, Figure S4b), both intensive Ca 2p and Ca 2s peaks appeared in the spectra. The Ca/P ratio was determined to be 1.5, which is lower than the normal value of 1.67.⁴¹ This result may be attributed to the fact that CPPs contain a portion of P element, causing the content of P to increase in the total sample. Thus, the Ca/P ratio was low.

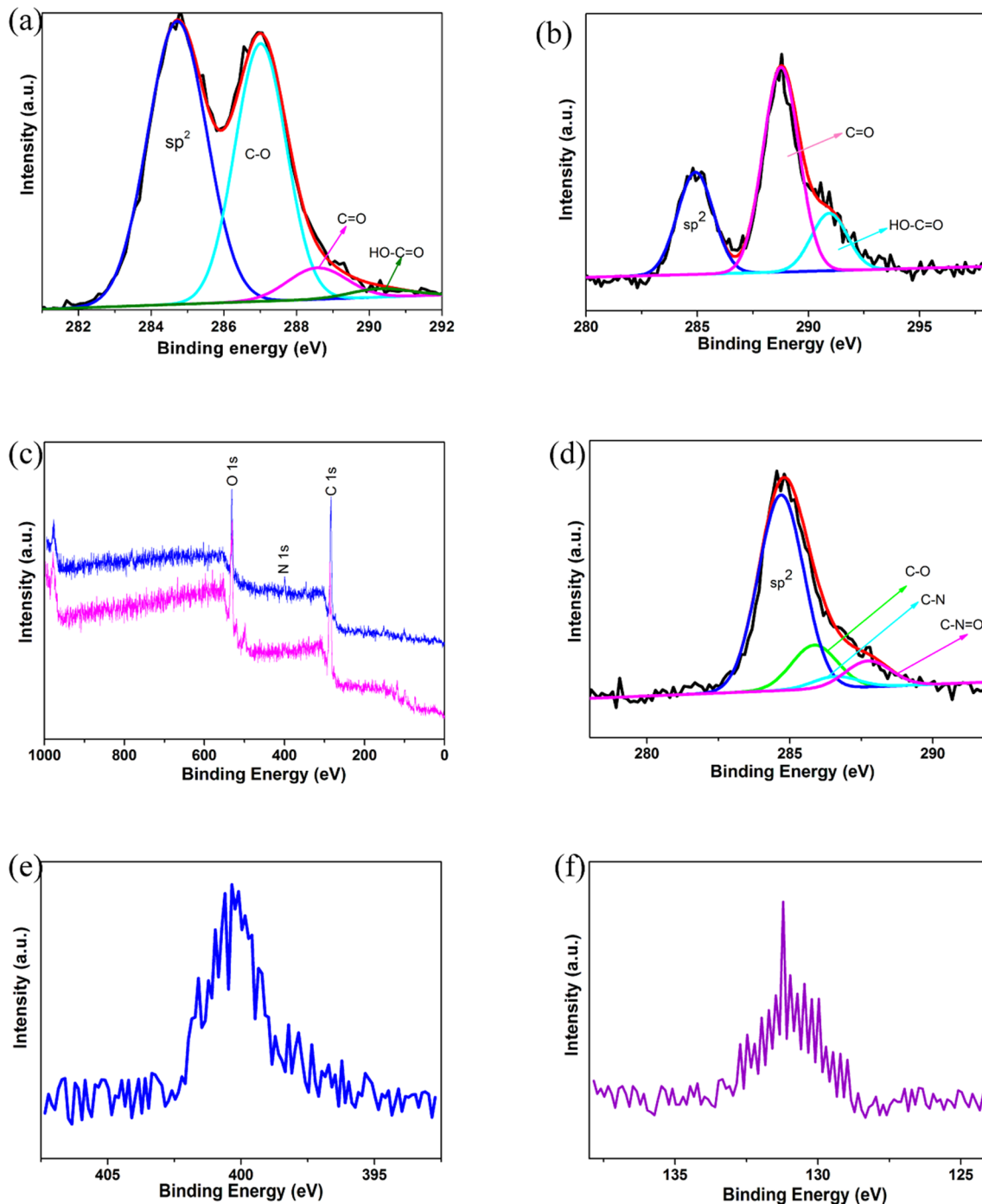


Figure 3. XPS spectra of C 1s for GO (a) and CGO (b), the survey spectra of CGO and CGO–CPPs (c), and the XPS spectra of C 1s (d), N 1s (e), and P 2p (f) for CGO–CPPs.

The XRD patterns of CGO–CPPs with different soaking times are displayed in Figure 8. After 1 day of immersion, two peaks at 25.8° and 32° were indexed as the (002) and (112) planes of HA, respectively. When the soaking time was prolonged to 3 days, the peak intensity at 32° increased, and more new peaks appeared at 39.8° , 49.4° , 53.1° , and 61.6° , which can be assigned to the (310), (213), (004), and (214) planes,^{42,43} respectively. These characteristic peaks are consistent with the standard diffraction pattern of HA (JCPDF 09–432), except for the peak of CGO–CPPs at 23° .²⁸ For comparison, the XRD pattern of CGO did not show the characteristic peaks of HA, except for the CGO peaks after

1 day of immersion (Supporting Information, Figure S5b). For the 3 day sample, two peaks located at 10.8° and 42° can be indexed as the (100) and (302) planes of HA (Supporting Information, Figure S5c), respectively.

The above-mentioned results were further confirmed by FTIR characterization. Figure 9 gives the FTIR spectra of the CGO–CPPs after being soaked in SBF for different periods. Obviously, all spectra presented characteristic absorption bands of HA, aside from the CGO–CPPs band at 1650 cm^{-1} and the stretching vibration of CO_3^{2-} at 1410 cm^{-1} .⁴⁴ The absorption bands at 1030 and 962 cm^{-1} corresponded to the symmetric stretching mode of PO_4^{3-} , whereas those at 605 and 566 cm^{-1}

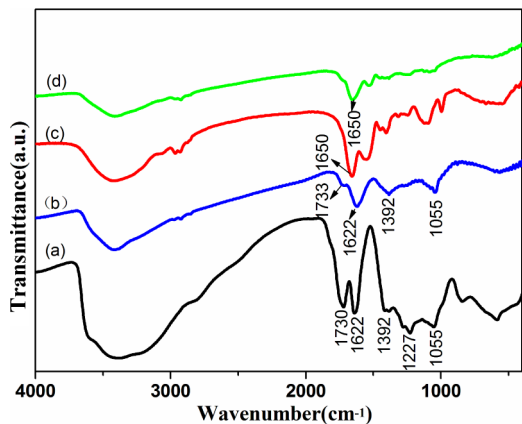


Figure 4. FTIR spectra of GO (a), CGO (b), CPPs (c), and CGO–CPPs (d).

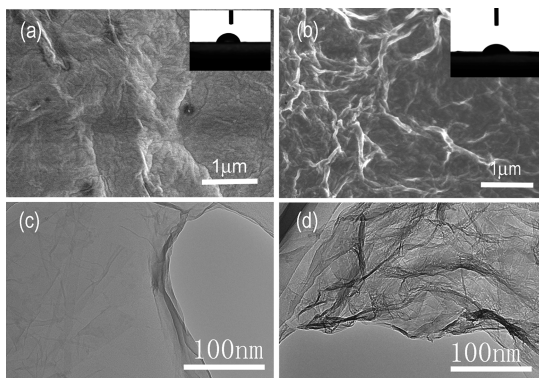


Figure 5. SEM and WCA images of CGO (a) and CGO–CPPs (b) and TEM images of CGO (c) and CGO–CPPs (d).

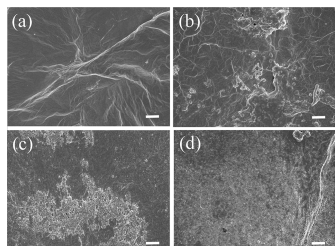


Figure 6. SEM images of CGO (a,b) and CGO–CPPs (c,d) after being immersed in SBF for 1 and 3 days, respectively (scale bar = 1 μ m).

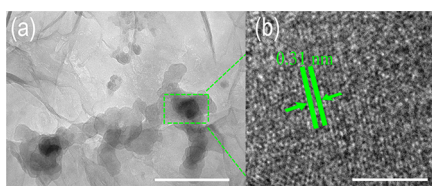


Figure 7. (a) TEM (scale bar = 200 nm) and (b) HRTEM (scale bar = 5 nm) images of sample after being immersed in SBF for 3 days.

corresponded to the asymmetric bending vibration of PO_4^{3-} .⁴⁵ The results prove the successful formation of HA on the composite after being soaked in SBF by mimetic mineralization.

Thermal Stability. TGA analyses were performed to confirm the weight change of HA in the CGO–CPPs composite upon incubation in the SBF solution for different

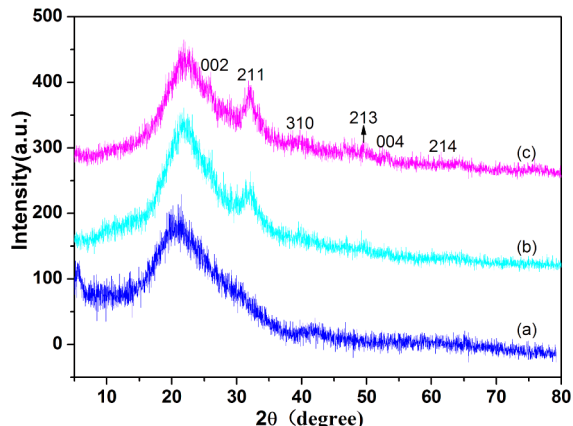


Figure 8. XRD patterns of CGO–CPPs after being immersed in SBF for 0 (a), 1 (b), and 3 days (c).

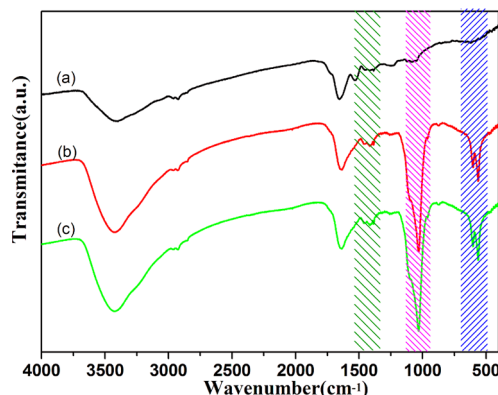


Figure 9. FTIR spectra of CGO–CPPs after being soaked in SBF for 0 (a), 1 (b), and 3 days (c), respectively. The characteristic peaks of CO_3^{2-} and PO_4^{3-} groups are marked by rectangle.

periods. The samples were heated to 1000 °C at a rate of 10 °C/min, and the results are shown in Figure 10. The thermogram of CPPs showed that the weight loss of the sample was ~76% when the temperature reached 620 °C. At the same temperature, the weight loss of CGO–CPPs was reduced to 56%, indicating that the introduction of CGO enhanced the thermal stability of CPPs. This finding may be

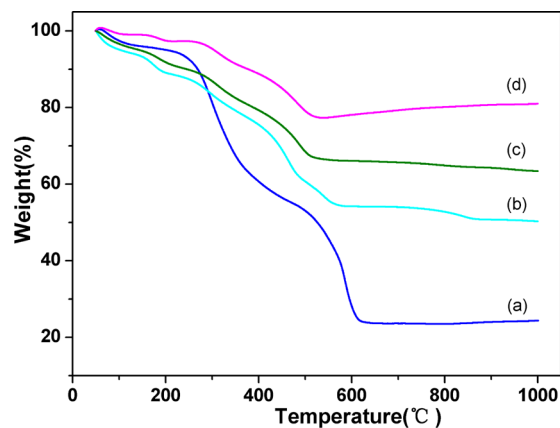


Figure 10. TGA curves of CPPs (a), CGO–CPPs (b), and CGO–CPPs after being immersed in SBF for 1 day (c) and 3 days (d), respectively.

attributed to the fact that CGO is reduced to graphene at high temperatures,^{45,46} which displays better thermal stability than CGO. For the samples immersed in SBF for 1 and 3 days, the weight losses were 33 and 22% at 620 °C, respectively. Compared with CGO–CPPs, the enhancement of thermal stability after mineralization might be attributed to the electrostatic integration between HA and CGO–CPPs and the high thermal stability of HA.^{47,48} The obvious decrease in weight loss illustrated that the deposited content of HA increased largely as the incubated time was prolonged.

Growth Mechanism of HA on CGO–CPPs. According to the above discussion and analysis, a possible mechanism for the formation of HA on CGO–CPPs was proposed (Figure 11).

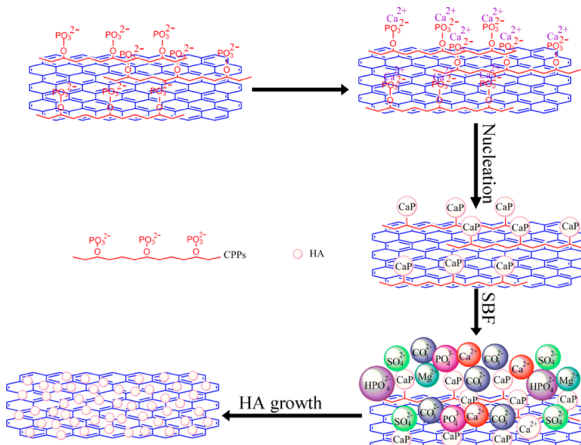


Figure 11. Growth mechanism of HA coating on CGO–CPPs.

After 1 day of immersion in SBF, numerous tiny HA particles appeared on the surface of CGO–CPPs. However, no deposit was observed in CGO. Therefore, phosphorus clusters of CPPs have important functions in accelerating HA formation and in shortening mineralization time. Specifically, phosphorus clusters contain negative charges, making them easily integrate with the positively charged calcium ions through electrostatic integration. New nucleation sites were created when calcium ions bound to phosphorus groups. PO_4^{3-} and OH^- groups were absorbed around the nucleation sites; hence, HA particles formed and anchored on the surface of the composite. As the mineralization time was prolonged, HA particles almost covered the entire surface of CGO–CPPs and formed an HA coating.

CONCLUSIONS

Biomimetic mineralization, as an effective way of designing novel composite materials by mimicking the biological process, has aroused considerable interest. Proteins and amino acids containing acidic amino-acid residues (e.g., aspartic acid and glutamic acid residues) are commonly used as active substances for HA biomimetic mineralization. Compared with proteins and amino acids, CPPs contain not only acidic amino acid residues but also large quantities of phosphate groups, providing more active sites for HA biomimetic mineralization. In this work, CPPs bound with CGO to form the biocomposite scaffold of CGO–CPPs and improve the bioactivity of CGO. Compared with the pristine CGO, bioactive CPPs have numerous phosphoserine groups and can be employed as nucleation and growth sites for accelerating the formation of HA and for shortening the

mineralization time. The synthesized HA on the surface of the composite by biomimetic mineralization had a similar composition to the natural bone, demonstrating that the obtained composite can provide binding sites for host tissues and enhance bone binding ability. Some potential applications of the CGO–CPPs composite in tissue engineering are in progress.

ASSOCIATED CONTENT

Supporting Information

EDX images of CGO, and CGO–CPPs, SEM images of CGO–CPPs incubated in SBF for 1 and 3 days, SAED image of HA and EDX image of CGO–CPPs/HA, XPS survey spectra of CGO–CPPs incubated in SBF for 0 and 3 days, and XRD patterns of CGO incubated in SBF for 0, 1, and 3 days. This material is available free of charge via the Internet at <http://pubs.acs.org>.

AUTHOR INFORMATION

Corresponding Author

*Tel: +86 931 4968076. Fax: +86 931 8277088. E-mail: jwang@licp.ac.cn (J.W.); sryang@licp.ac.cn (S.Y.).

Notes

The authors declare no competing financial interest.

ACKNOWLEDGMENTS

We thank the National Natural Science Foundation of China (grant nos. 51075384 and 51205385) and “Top Hundred Talents Program” of Chinese Academy of Sciences for financial support.

REFERENCES

- (1) Cao, H. Q.; Zhang, L.; Zheng, H.; Wang, Z. Hydroxyapatite Nanocrystals for Biomedical Applications. *J. Phys. Chem. C* **2010**, *114*, 18352–18357.
- (2) Costa, D. O.; Dixon, S. J.; Rizkalla, A. S. One- and Three-Dimensional Growth of Hydroxyapatite Nanowires during Sol-Gel-Hydrothermal Synthesis. *ACS Appl. Mater. Interfaces* **2012**, *4*, 1490–1499.
- (3) Tan, Q. G.; Zhang, K.; Gu, S. Y.; Ren, J. Mineralization of Surfactant Functionalized Multi-Walled Carbon Nanotubes (MWNTs) to Prepare Hydroxyapatite/MWNTs Nano-hybrid. *Appl. Surf. Sci.* **2009**, *255*, 7036–7039.
- (4) Carradó, A. Structural, Microstructural, and Residual Stress Investigations of Plasma-Sprayed Hydroxyapatite on Ti-6Al-4V. *ACS Appl. Mater. Interfaces* **2010**, *2*, 561–565.
- (5) Huang, J.; Best, S. M.; Bonfield, W.; Buckland, T. Development and Characterization of Titanium-Containing Hydroxyapatite for Medical Applications. *Acta Biomater.* **2010**, *6*, 241–249.
- (6) Wang, H.; Eliaz, N.; Xiang, Z.; Hsu, H. P.; Spector, M.; Hobbs, L. W. Early Bone Apposition in Vivo on Plasma-Sprayed and Electrochemically Deposited Hydroxyapatite Coatings on Titanium Alloy. *Biomaterials* **2006**, *27*, 4192–4203.
- (7) Lobo, A. O.; Corat, M. A. F.; Ramos, S. C.; Matsushima, J. T.; Granato, A. E. C.; Pacheco-Soares, C.; Corat, E. J. Fast Preparation of Hydroxyapatite/Superhydrophilic Vertically Aligned Multiwalled Carbon Nanotube Composites for Bioactive Application. *Langmuir* **2010**, *26*, 18308–18314.
- (8) Rodríguez-Valencia, C.; Rial, L.; Serra, J.; González, P.; Rodríguez-González, J. B.; Mateo-Mateo, C.; Correa-Duarte, M. A. Tuning the Biomineralization Process for Controlling the Nucleation and Oriented Growth of Ca-P Crystals onto Functionalized Carbon Nanotubes. *J. Phys. Chem. C* **2012**, *116*, 3400–3404.
- (9) Goncalves, G.; Cruz, S. M. A.; Ramalho, A.; Gracio, J.; Marques, P. A. A. P. Graphene Oxide Versus Functionalized Carbon Nanotubes

- As a Reinforcing Agent in a PMMA/HA Bone Cement. *Nanoscale* **2012**, *4*, 2937–2945.
- (10) Puleo, D. A.; Nanci, A. Understanding and Controlling the Bone–Implant Interface. *Biomaterials* **1999**, *20*, 2311–2321.
 - (11) Weng, J.; Liu, Q.; Wolke, J. G. C.; Zhang, X.; de Groot, K. Formation and Characteristics of the Apatite Layer on Plasma-Sprayed Hydroxyapatite Coatings in Simulated Body Fluid. *Biomaterials* **1997**, *18*, 1027–1035.
 - (12) Sung, H. W.; Chang, Y.; Liang, I. L.; Chang, W. H.; Chen, Y. C. Fixation of Biological Tissues With a Naturally Occurring Crosslinking Agent: Fixation Rate and Effects of pH, Temperature, and Initial Fixative Concentration. *J.Biomed. Mater. Res.* **2000**, *52*, 77–87.
 - (13) Yang, C. W.; Lui, T. S. Kinetics of Hydrothermal Crystallization under Saturated Steam Pressure and the Self-Healing Effect by Nanocrystallite for Hydroxyapatite Coatings. *Acta. Biomater.* **2009**, *5*, 2728–2737.
 - (14) Zhao, H. X.; Dong, W. J.; Zheng, Y. Y.; Liu, A. P.; Yao, J. M.; Li, C. R.; Tang, W. H.; Chen, B. Y.; Wang, G.; Shi, Z. The Structural and Biological Properties of Hydroxyapatite-modified Titanate Nanowire Scaffolds. *Biomaterials* **2011**, *32*, 5837–5846.
 - (15) Mobasherpour, I.; Heshajin, M. S.; Kazemzadeh, A.; Zakeri, M. Synthesis of Nanocrystalline Hydroxyapatite by Using Precipitation Method. *J. Alloy. Compd.* **2007**, *430*, 330–333.
 - (16) Weng, J.; Liu, X.; Zhang, X.; Ma, Z.; Ji, X.; Zyman, Z. Further Studies on the Plasma-Sprayed Amorphous Phase in Hydroxyapatite Coatings and Its Deamorphization. *Biomaterials* **1993**, *14*, 578–582.
 - (17) Li, Y. P.; Thula, T. T.; Jee, S.; Perkins, S. L.; Aparicio, C.; Douglas, E. P.; Gower, L. B. Biomimetic Mineralization of Woven Bone-Like Nanocomposites: Role of Collagen Cross-Links. *Biomacromolecules* **2011**, *13*, 49–59.
 - (18) Huang, J. J.; Liu, G.; Song, C. Y.; Saiz, E.; Tomsia, A. P. Role of Molecular Chemistry of Degradable pHEMA Hydrogels in Three-Dimensional Biomimetic Mineralization. *Chem. Mater.* **2012**, *24*, 1331–1337.
 - (19) Ravichandran, R.; Ng, C. C.; Liao, S.; Pliszka, D.; Raghunath, M.; Ramakrishna, S.; Chan, C. K. Biomimetic Surface Modification of Titanium Surfaces for Early Cell Capture by Advanced Electrospinning. *Biomed. Mater.* **2012**, *7*, 015001.
 - (20) Wei, G.; Zhang, J. T.; Xie, L.; Jandt, K. D. Biomimetic Growth of Hydroxyapatite on Super Water-Soluble Carbon Nanotube-Protein Hybrid Nanofibers. *Carbon* **2011**, *49*, 2216–2226.
 - (21) Chien, C. Y.; Liu, T. Y.; Kuo, W. H.; Wang, M. J.; Tsai, W. B. Dopamine-Assisted Immobilization of Hydroxyapatite Nanoparticles and RGD Peptides to Improve the Osteoconductivity of Titanium. *J. Biomed. Mater. Res.* **2012**, *101*, 740–747.
 - (22) Ryu, J. K.; Ku, S. H.; Lee, M.; Park, C. B. Mussel-Inspired Polydopamine Coating as a Universal Route to Hydroxyapatite Crystallization. *Soft Mater.* **2011**, *7*, 7201–7206.
 - (23) Palazzo, B.; Walsh, D.; Iafisco, M.; Foresti, E.; Bertinetti, L.; Martra, G.; Bianchi, C. L.; Cappelletti, G.; Roveri, N. Amino Acid Synergistic Effect on Structure, Morphology and Surface Properties of Biomimetic Apatite Nanocrystals. *Acta. Biomater.* **2009**, *5*, 1241–1252.
 - (24) Kokubo, T.; Takadama, H. How Useful is SBF in Predicting in Vivo Bone Bioactivity? *Biomaterials* **2006**, *27*, 2907–2915.
 - (25) Yao, J.; Sun, Y.; Yang, M.; Duan, Y. Chemistry, Physics and Biology of Graphene-Based Nanomaterials: New Horizons for Sensing, Imaging and Medicine. *J. Mater. Chem.* **2012**, *22*, 14313–14329.
 - (26) Liu, H.; Xi, P.; Xie, G.; Shi, Y.; Hou, F.; Huang, L.; Chen, F.; Zeng, Z.; Shao, C.; Wang, J. Simultaneous Reduction and Surface Functionalization of Graphene Oxide for Hydroxyapatite Mineralization. *J. Phys. Chem. C* **2012**, *116*, 3334–3341.
 - (27) Cui, W. G.; Li, X. H.; Xie, C. Y.; Zhuang, H. H.; Zhou, S. B.; Weng, J. Hydroxyapatite Nucleation and Growth Mechanism on Electrospun Fibers Functionalized with Different Chemical Groups and Their Combinations. *Biomaterials* **2010**, *31*, 4620–4629.
 - (28) Shchukin, D. G.; Sukhorukov, G. B.; Möhwald, H. Biomimetic Fabrication of Nanoengineered Hydroxyapatite/Polyelectrolyte Composite Shell. *Chem. Mater.* **2003**, *15*, 3947–3950.
 - (29) Phelan, M.; Aherne, A.; FitzGerald, R. J.; O'Brien, N. M. Casein-Derived Bioactive Peptides: Biological Effects, Industrial Uses, Safety Aspects and Regulatory Status. *Int. Dairy. J.* **2009**, *19*, 643–654.
 - (30) Silva, S. V.; Malcata, F. X. Caseins as Source of Bioactive Peptides. *Int. Dairy. J.* **2005**, *15*, 1–15.
 - (31) Hummers, W. S.; Offeman, R. E. Preparation of Graphitic Oxide. *J. Am. Chem. Soc.* **1958**, *80*, 1339–1339.
 - (32) Sun, X.; Liu, Z.; Welsher, K.; Robinson, J. T.; Goodwin, A.; Zaric, S.; Dai, H. Nano-Graphene Oxide for Cellular Imaging and Drug Delivery. *Nano. Res.* **2008**, *1*, 203–212.
 - (33) Peng, H. D.; Meng, L. J.; Lu, Q. H.; Dong, S.; Fei, Z. F.; Dyson, P. J. Fabrication of Reduced Graphene Oxide Hybrid Materials that Exhibit Strong Fluorescence. *J. Mater. Chem.* **2012**, *22*, 14868–14873.
 - (34) Shang, J. Z.; Ma, L.; Li, J. W.; Ai, W.; Yu, T.; Gurzadyan, G. G. The Origin of Fluorescence from Graphene Oxide. *Sci. Rep.* **2012**, *2*, 792.
 - (35) Yoonessi, M.; Shi, Y.; Scheiman, D. A.; Lebron-Colon, M.; Tigelaar, D. M.; Weiss, R. A.; Meador, M. A. Graphene Polyimide Nanocomposites; Thermal, Mechanical, and High-Temperature Shape Memory Effects. *ACS Nano* **2012**, *6*, 7644–7655.
 - (36) Li, L.; Chan, C. M.; Weng, L. T. Effects of the Sequence Distribution of Poly(acrylonitrile–butadiene) Copolymers on the Surface Chemical Composition As Determined by XPS and Dynamic Contact Angle Measurements. *Macromolecules* **1997**, *30*, 3698–3700.
 - (37) Kaminska, I.; Das, M. R.; Coffinier, Y.; Niedziolka-Jonsson, J.; Sobczak, J.; Woisel, P.; Lyskawa, J.; Opallo, M.; Boukherroub, R.; Szunerits, S. Reduction and Functionalization of Graphene Oxide Sheets Using Biomimetic Dopamine Derivatives in One Step. *ACS. Appl. Mater. Interfaces* **2012**, *4*, 1016–1020.
 - (38) Kim, S. N.; Kuang, Z. F.; Slocik, J. M.; Jones, S. E.; Cui, Y.; Farmer, B. L.; McAlpine, M. C.; Naik, R. R. Preferential Binding of Peptides to Graphene Edges and Planes. *J. Am. Chem. Soc.* **2011**, *133*, 14480–14483.
 - (39) Wang, H. B.; Zhang, Q.; Chen, T. T.; Ge, J.; Yu, R. Q. Graphene Oxide–Peptide Conjugate as an Intracellular Protease Sensor for Caspase-3 Activation Imaging in Live Cells. *Angew. Chem., Int. Ed.* **2011**, *50*, 7065–7069.
 - (40) Li, H.; Khor, K. A.; Cheang, P. Titanium Dioxide Reinforced Hydroxyapatite Coatings Deposited by High Velocity Oxy-Fuel (HVOF) Spray. *Biomaterials* **2004**, *25*, 3463–3471.
 - (41) Palusziewicz, C.; Blažewicz, M.; Podporska, J.; Gumula, T. Nucleation of Hydroxyapatite Layer on Wollastonite Material Surface: FTIR Studies. *Vib. Spectrosc.* **2008**, *48*, 263–268.
 - (42) Eraković, S.; Janković, A.; Veljović, D.; Palcevskis, E.; Mitrić, M.; Stevanović, T.; Janačković, D.; Mišković-Stanković, V. Corrosion Stability and Bioactivity in Simulated Body Fluid of Silver/Hydroxyapatite and Silver/Hydroxyapatite/Lignin Coatings on Titanium Obtained by Electrophoretic Deposition. *J. Phys. Chem. B* **2012**, *117*, 1633–1643.
 - (43) Cao, M. H.; Wang, Y. H.; Guo, C. X.; Qi, Y. J.; Hu, C. W. Preparation of Ultrahigh-Aspect-Ratio Hydroxyapatite Nanofibers in Reverse Micelles under Hydrothermal Conditions. *Langmuir* **2004**, *20*, 4784–4786.
 - (44) Wang, X. J.; Li, Y. B.; Wei, J.; de Groot, K. Development of Biomimetic Nano-Hydroxyapatite/Poly(hexamethylene adipamide) Composites. *Biomaterials* **2002**, *23*, 4787–4791.
 - (45) Hsiao, M. C.; Liao, S. H.; Yen, M. Y.; Liu, P. I.; Pu, N. W.; Wang, C. A.; Ma, C. C. M. Preparation of Covalently Functionalized Graphene Using Residual Oxygen-Containing Functional Groups. *ACS Appl. Mater. Interfaces* **2010**, *2*, 3092–3099.
 - (46) Jung, I.; Vaupel, M.; Pelton, M.; Piner, R.; Dikin, D. A.; Stankovich, S.; An, J.; Ruoff, R. S. Characterization of Thermally Reduced Graphene Oxide by Imaging Ellipsometry. *J. Phys. Chem. C* **2008**, *112*, 8499–8506.
 - (47) Li, M.; Wang, Y. B.; Liu, Q.; Li, Q. H.; Cheng, Y.; Zheng, Y. F.; Xi, Q. F.; Wei, S. C. In Situ Synthesis and Biocompatibility of Nano Hydroxyapatite on Pristine and Chitosan Functionalized Graphene Oxide. *J. Mater. Chem. B* **2013**, *1*, 275–284.

- (48) Ashok, M.; Meenakshi Sundaram, N.; Narayana Kalkura, S. Crystallization of Hydroxyapatite at Physiological Temperature. *Mater. Lett.* **2003**, *57*, 2066–2070.